2017-12-26

Rlim-Dependent and -Independent Pathways for X Chromosome Inactivation in Female ESCs

Feng Wang
University of Massachusetts Medical School

Et al.

Cell Reports

Rlim-Dependent and -Independent Pathways for X Chromosome Inactivation in Female ESCs

Graphical Abstract

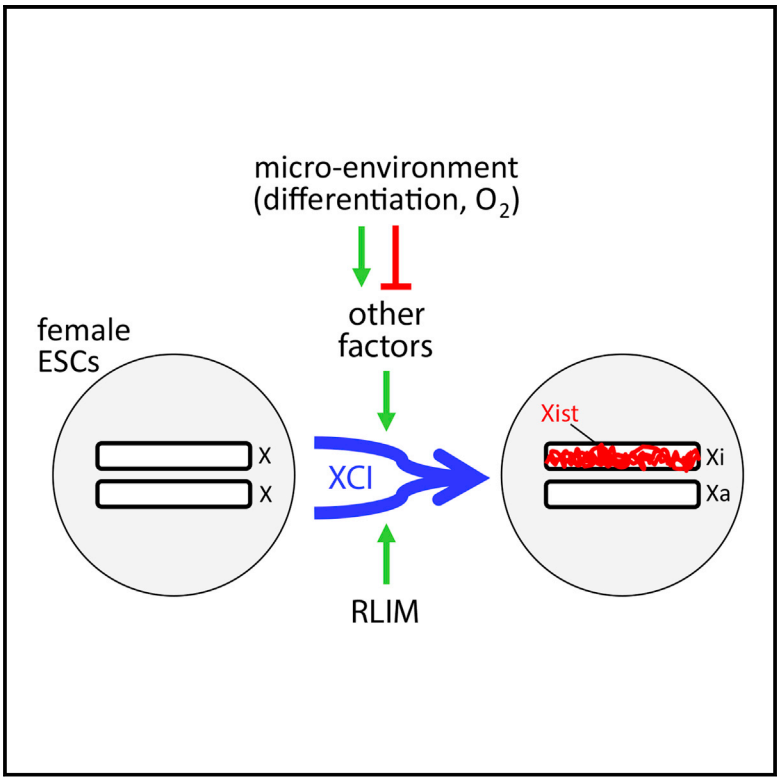

Authors

Feng Wang, Kurtis N. McCannell, Ana Bošković, ..., Oliver J. Rando, Thomas G. Fazzio, Ingolf Bach

Correspondence

ingolf.bach@umassmed.edu

In Brief

Embryonic stem cells are widely used for investigating X chromosome inactivation, the silencing of one X chromosome in females. Wang et al. show that this process is driven by two independent pathways, one that requires the ubiquitin ligase *Rlim* and another that functions independently of *Rlim* and is sensitive to environmental conditions.

Highlights

- rXCI in epiblast cells does not require *Rlim*
- XCI in RA-differentiated female ESCs depends on *Rlim*
- *Rlim*-independent XCI occurs in EB-differentiated female ESCs
- Culturing ESCs under physiological O_2 levels promotes *Rlim*-independent XCI

Data and Software Availability

GSE101838

Wang et al., 2017, Cell Reports *21*, 3691–3699
December 26, 2017
https://doi.org/10.1016/j.celrep.2017.12.004

CellPress

Cell Reports
Report

Rlim-Dependent and -Independent Pathways for X Chromosome Inactivation in Female ESCs

Feng Wang,[1] Kurtis N. McCannell,[1] Ana Bošković,[2] Xiaochun Zhu,[1] JongDae Shin,[1,6] Jun Yu,[1] Judith Gallant,[3] Meg Byron,[3] Jeanne B. Lawrence,[3] Lihua J. Zhu,[1,4,5] Stephen N. Jones,[3,7] Oliver J. Rando,[2] Thomas G. Fazzio,[1,4] and Ingolf Bach[1,4,8,*]

[1]Department of Molecular, Cell and Cancer Biology, University of Massachusetts Medical School, Worcester, MA 01605, USA
[2]Department of Biochemistry and Molecular Pharmacology, University of Massachusetts Medical School, Worcester, MA 01605, USA
[3]Department of Cell and Developmental Biology, University of Massachusetts Medical School, Worcester, MA 01605, USA
[4]Program in Molecular Medicine, University of Massachusetts Medical School, Worcester, MA 01605, USA
[5]Program in Bioinformatics and Integrative Biology, University of Massachusetts Medical School, Worcester, MA 01605, USA
[6]Present address: Department of Cell Biology, College of Medicine, Konyang University, Daejeon, Korea
[7]Present address: Frederick National Laboratory for Cancer Research, Frederick, MD 21702, USA
[8]Lead Contact
*Correspondence: ingolf.bach@umassmed.edu
https://doi.org/10.1016/j.celrep.2017.12.004

SUMMARY

During female mouse embryogenesis, two forms of X chromosome inactivation (XCI) ensure dosage compensation from sex chromosomes. Beginning at the four-cell stage, imprinted XCI (iXCI) exclusively silences the paternal X (Xp), and this pattern is maintained in extraembryonic cell types. Epiblast cells, which give rise to the embryo proper, reactivate the Xp (XCR) and undergo a random form of XCI (rXCI) around implantation. Both iXCI and rXCI depend on the long non-coding RNA *Xist*. The ubiquitin ligase RLIM is required for iXCI *in vivo* and occupies a central role in current models of rXCI. Here, we demonstrate the existence of *Rlim*-dependent and *Rlim*-independent pathways for rXCI in differentiating female ESCs. Upon uncoupling these pathways, we find more efficient *Rlim*-independent XCI in ESCs cultured under physiological oxygen conditions. Our results revise current models of rXCI and suggest that caution must be taken when comparing XCI studies in ESCs and mice.

INTRODUCTION

Female mammalian embryogenesis and reproduction critically depend on a process called X chromosome inactivation (XCI), which silences one of the two sex chromosomes to achieve dosage compensation. XCI serves as a paradigm to study the epigenetic regulation, whereby gene expression states are maintained independent of DNA sequence. In mice, an imprinted form of XCI (iXCI) is initiated in embryos at the 4-cell stage, silencing exclusively the paternal X (Xp), and this XCI pattern is maintained in extraembryonic tissues. However, epiblast cells, which give rise to the embryo proper, experience a major epigenetic switch around implantation: these cells reactivate the Xp and undergo a random form of XCI (rXCI), in which the Xp or the maternal X (Xm) is inactivated in each cell with equal probability (Payer, 2016). Both forms of XCI require the long non-coding *Xist* RNA, which forms clouds on the inactive X chromosome (Xi) from which it is transcribed, leading to X silencing. The X-linked gene *Rlim* (also known as *Rnf12*) has emerged as a critical mediator of *Xist* activity. *Rlim* encodes a ubiquitin ligase (E3) (Ostendorff et al., 2002) that is involved in transcriptional regulation (Bach et al., 1999; Gontan et al., 2012; Güngör et al., 2007) and shuttles between the nucleus and the cytoplasm (Jiao et al., 2013). In mice, a maternally transmitted *Rlim* knockout (KO) allele (Δ_m) results in early lethality of female embryos in a sex-specific parent-of-origin effect due to a failure to maintain iXCI and *Xist* clouds (Shin et al., 2010; Wang et al., 2016). In contrast, loss of *Rlim* in female epiblast cells has minimal effect on the rXCI process. RLIM protein levels are downregulated specifically in epiblast cells of implanting embryos, consistent with the lack of rXCI phenotype in *Rlim* mutant females (Shin et al., 2014). These data identify *Rlim*-dependent and *Rlim*-independent mechanisms of XCI *in vivo* that separately act in pre-implantation embryos and epiblasts, respectively. However, *Rlim* is crucial for XCI in female embryonic stem cells (ESCs) differentiated in culture (Barakat et al., 2011, 2014).

To further investigate mechanisms of rXCI, we generated female ESCs with a homozygous *Rlim*KO. We found that these cells undergo XCI *in vivo* but that XCI *in vitro* is strongly influenced by culture conditions, including both method of differentiation and O_2 levels. Our results demonstrate *Rlim*-dependent and *Rlim*-independent pathways for XCI exist in ESCs and, together with published data, profoundly change current models of X dosage compensation.

RESULTS

Female ESCs Lacking RLIM Undergo XCI *In Vivo*

Genetic evidence indicates that iXCI in female pre-implantation embryos requires RLIM but that activation of *Xist* during rXCI in the female epiblast is *Rlim*-independent (Shin et al., 2010, 2014). *Xist* clouds form specifically in the inner cell mass (ICM) of female blastocyst outgrowths with a maternal *Rlim* deletion (Δ_m) (Shin et al., 2010), consistent with a critical role for RLIM

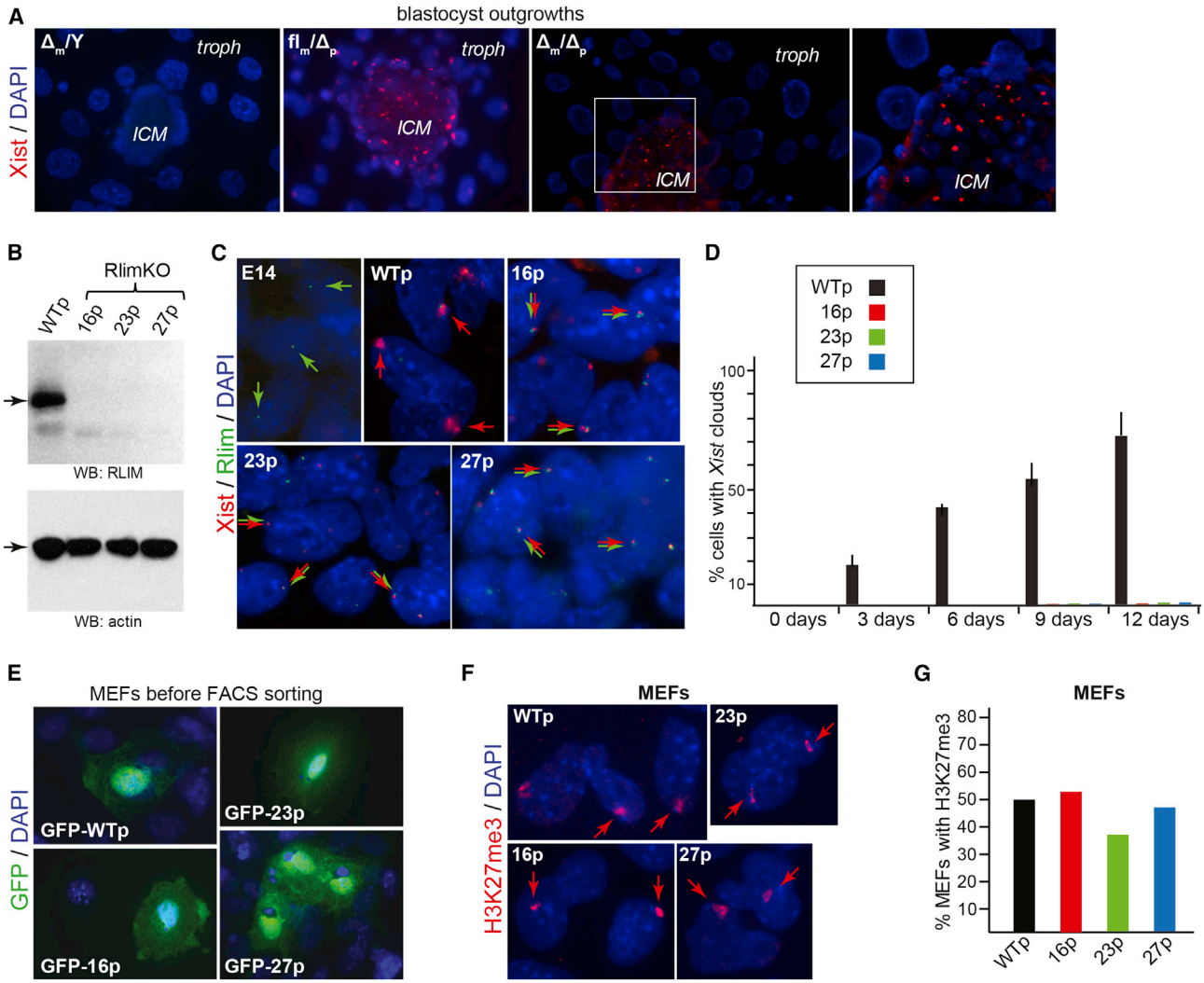

Figure 1. *Rlim*-Independent XCI in Female ESCs *In Vivo*

(A) Development of *Xist* clouds in ICM of female blastocyst outgrowths lacking maternal and embryonic RLIM. RNA FISH on E4 blastocyst outgrowths cultured for 72 hr using *Xist* as the probe. Embryos were generated by crossing Δ/Y males with either SC-cKO$_m$/Δ$_p$ or fl/fl females. The boxed area (Δ$_m$/Δ$_p$ embryo) is shown in higher magnification in the right panel. Focus in images is on cells in the ICM. Embryos were genotyped after image recording.

(B) Generation of female *Rlim*KO ESC lines via CRISPR/Cas9. Western blot of undifferentiated WTp and *Rlim*KOp lines using antibodies against RLIM (top) or β-actin (bottom).

(C) XCI upon RA differentiation of ESCs is *Rlim*-dependent. RNA FISH on day 6 RA-differentiated ESCs using *Xist* (red) and *Rlim* (green) as probes. There are side-by-side *Xist* and *Rlim* transcription foci but no *Xist* clouds in *Rlim*KO ESCs.

(D) XCI profile in ESCs differentiated by RA for up to 12 days. Data reflect two independent experiments, with >500 cells counted for each ESC line and time point. Error bars indicate SEM.

(E) Approximately 12–15 undifferentiated GFP-tagged ESCs were microinjected into E3.5 blastocysts, which were surgically placed into the uteri of pseudo-pregnant females. MEFs were prepared from E12.5 embryos and stained with GFP antibodies.

(F) FACS-sorted WT and KO MEFs were stained with antibodies against H3K27me3. Arrows show H3K27me3 foci marking the Xi.

(G) Summary of H3K27me3 foci in (F); n > 150 cells each.

See also Figure S1.

in iXCI but not rXCI. To exclude any influence of RLIM on rXCI, we examined Δ$_m$/Δ$_p$ (paternally transmitted *Rlim*KO allele) female blastocysts generated by crossing Δ/Y males with Sox2-Cre (SC)-cKO$_m$ (conditional KO of a maternally transmitted *Rlim*fl allele)/Δ$_p$ dams, which lack RLIM in both somatic tissues and germline (Wang et al., 2016). E4 blastocysts generated by this cross were cultured for 3 days and analyzed by RNA fluorescence *in situ* hybridization (FISH). *Xist* clouds were readily detectable specifically in cells of the ICM in female Δ/Δ blastocyst outgrowths (Figure 1A), consistent with *Rlim*-independent induction of rXCI *in vivo*.

Newly isolated primary female ESCs that lack RLIM activate *Xist* and form *Xist* clouds upon differentiation *in vitro* (Shin et al., 2010, 2014). However, in a female ESC line with a

homozygous *Rlim* KO (Rnf12KO), XCI was blocked upon ESC differentiation (Barakat et al., 2011), suggesting that XCI is induced in a context-dependent manner. Because primary female *Rlim*KO ESCs proved unstable upon prolonged culture, to investigate mechanisms of XCI, we generated three independent ESC lines lacking RLIM via CRISPR/Cas9 technology (Figure 1B) using the established mouse PGK12.1 female ESC model (Norris et al., 1994). Sequencing confirmed homozygous frameshift mutations in exon 3, the first coding exon in *Rlim* (Figure S1A). We named these lines *Rlim*16p, *Rlim*23p, and *Rlim*27p, reflecting the amino acid position where each frameshift occurred, as well as the ESC origin (where p indicates PGK12.1). Consistent with published results (Barakat et al., 2011), differentiation upon treatment with retinoic acid (RA) showed that XCI was *Rlim*-dependent, because development of *Xist* clouds and H3K27me3 foci was inhibited in *Rlim*KO ESCs, even after differentiating cells for 12 days (Figures 1C, 1D, S1B, and S1C). As previously reported (Barakat et al., 2011), we observed sporadic clusters of a few cells that displayed H3K27me3 foci in all KO lines (data not shown), indicating that *Rlim*KO ESCs have the ability to undergo XCI but do so at a very low rate. To further investigate the potential of *Rlim*KO ESCs for XCI, we examined their XCI capability *in vivo*. To allow lineage tracing, we used lentiviral infections to generate wild-type (WT) and *Rlim*KO ESC lines stably expressing GFP (lentivirus pWPT-GFP, Addgene) (Figure S1D) (data not shown). Approximately 10–15 GFP-ESCs were microinjected in mouse pre-implantation embryos at E3.5. Injected embryos were surgically placed into the uteri of pseudo-pregnant females and allowed to develop, and mouse embryonic fibroblasts (MEFs) of E12.5 embryos were prepared and tested for GFP expression in immunocytochemistry (ICC) (Figure 1E). GFP-positive MEFs of independent embryos were isolated via fluorescence-activated cell sorting (FACS) (6 each for WTp and *Rlim*16p, 3 for *Rlim*23p, and 1 for *Rlim*27p), and similar fractions of GFP-positive versus GFP-negative MEFs obtained from individual embryos injected with *Rlim*16p or WTp ESCs were obtained (Figure S1E). Testing for signs of XCI, around 40%–50% of WT and KO GFP-MEFs developed H3K27me3 foci (Figures 1F and 1G), and co-staining revealed more than 90% of MEFs with H3K27me3 foci displayed overlapping Xist clouds (Figure S1F). In strand-specific reverse transcription (RT)-qPCR (ssRT-qPCR), we did not detect significant differences in *Xist* levels between *Rlim*KO and WT MEFs (Figure S1G) or between E10.5 female embryos with or without RLIM (fl_m [maternally transmitted *Rlim*fl allele]/Δ_p and SC-cKO_m/Δ_p, respectively) (Figure S1H). Combined, these data show that female ESCs lacking RLIM cannot undergo XCI upon RA differentiation but can do so in the embryo, suggesting that environmental conditions influence XCI.

Rlim-Dependent and -Independent XCI in ESCs *In Vitro*

Next, we compared XCI induced by RA differentiation with embryoid body (EB) differentiation in ESCs. Profiling protein expression in WT ESCs via western blotting showed low levels of OCT4 by day 3 of differentiation, confirming ESC differentiation, whereas levels of RLIM by day 6 were similar to those in undifferentiated ESCs (Figure 2A). ssRT-qPCR analyses revealed that day 6 EB-differentiated WTp ESCs displayed less than 3-fold increased *Xist* levels when compared to RA-differentiated WT cells (Figure 2B). However, *Xist* levels in EB-differentiated *Rlim*KO ESCs were >50-fold higher under EB differentiation relative to RA, with *Xist* clouds developing in a significant number of cells (Figures 2C and 2D). Combined, these results provide the first evidence of *Rlim*-independent XCI in an established female ESC line and show that differentiation conditions play a major role in *Rlim*-independent induction of *Xist*. Moreover, unlike in differentiating epiblast cells *in vivo* (Shin et al., 2014), differentiation of ESCs *in vitro* does not induce significant RLIM downregulation.

In another female ESC model, the *RlimKO* (Rnf12KO) resulted in complete inhibition of XCI, leading to far-reaching conclusions regarding *Rlim* function in rXCI (Barakat et al., 2011, 2014). Because these results did not match our results (Figure 2), we directly compared our *Rlim*KO ESC lines with the Rnf12KO cell line (Barakat et al., 2011). The Rnf12KO cell line was achieved via insertion of foreign DNA into the *Rlim* gene at a position that might allow expression of a truncated RLIM protein consisting of the N-terminal 340 amino acids (Figure S2A) (Jonkers et al., 2009). Western blots using two independent RLIM antibodies detected a prominent band migrating around 45 kDa (RLIM340) in these ESCs (Figures 3A and S2B). Because of their F121 ESC background, we refer to this ESC line as *Rlim*340f. In agreement with published results (Gontan et al., 2012), REX1 levels in *Rlim*340f ESCs were increased (Figure 3A). *Rlim*KOp ESCs displayed similar REX1 levels to those of WTp ESCs (Figure 3A), indicating that in PGK12.1 ESCs, RLIM is not solely responsible for regulating cellular REX1 levels. The predicted RLIM340 protein lacks the RING finger and nuclear export signal (NES) but retains part of the basic domain that mediates interactions with many substrate proteins, including REX1 (Figure S2A) (Gontan et al., 2012; Ostendorff et al., 2002). ICC on undifferentiated *Rlim*340f ESCs revealed predominantly nuclear localization of the truncated RLIM protein (Figure S2C), consistent with findings that RLIM lacking the NES is trapped in the nucleus (Jiao et al., 2013). Moreover, forced expression of Myc-tagged RLIM340 in *Rlim*KOp ESCs via transient transfections revealed accumulation of endogenous REX1 protein in nuclei of transfected cells (Figure 3B). However, in WT PGK12.1 cells, expression of Myc-RLIM340 did not lead to REX1 accumulation, suggesting that the presence of the partial basic domain is not able to block interactions between full-length RLIM and REX1.

To investigate the effects of RLIM340 expression on XCI, we induced frameshift mutations in *Rlim*340f ESCs via CRISPR/Cas9, using the same guide RNAs as for the *Rlim*KOp ESCs and yielding, in independent ESCs carrying a homozygous KO of RLIM340, lines *Rlim*53f and *Rlim*0f (Figures S2A) (data not shown). Analysis of these lines via western blot corroborated the KO and showed that the presence of RLIM340 did not significantly affect overall REX1 levels in undifferentiated ESCs (Figure S2D). However, ICC staining confirmed that RLIM340 was critical to trap REX1 in the nucleus, because nuclear REX1 was significantly reduced in both KO lines relative to the *Rlim*340f line (Figure 3C). Moreover, these KO ESCs performed XCI upon EB differentiation at a higher rate than Rlim340f cells, as measured by formation of *Xist* clouds (Figure 3D). Combined, these results indicate gain-of-function activity of the truncated

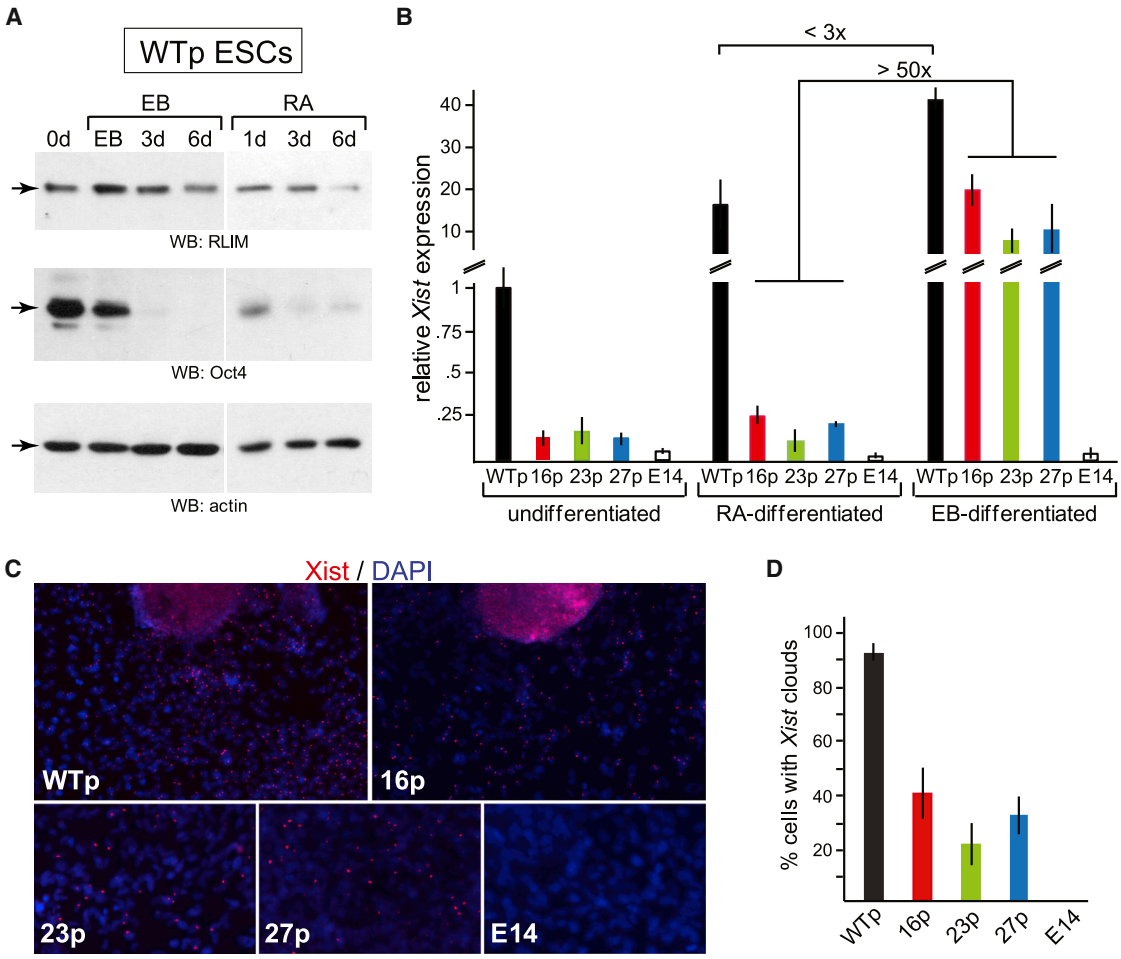

Figure 2. *Rlim*-Dependent and *Rlim*-Independent XCI Pathways Exist in ESCs

(A) WTp ESCs were split and *in vitro* differentiated in parallel by either EB or RA. Protein extracts were prepared at various time points during differentiation. The same western blot was hybridized with antibodies against RLIM, OCT4, and β-actin. Oct4 levels drop dramatically by day 3, whereas RLIM levels are not significantly downregulated by day 6.

(B) Comparison of *Xist* RNA levels in undifferentiated ESCs and after day 6 RA or EB differentiation via ssqRT-PCR (control, E14 male ESCs; *Xist* levels of undifferentiated WTp cells are set to 1). Data represent three independent experiments. *Xist* levels are <3× higher in EB-differentiated WTp ESCs when compared to RA differentiation but >50× for all *Rlim*KOp ESCs.

(C) Formation of *Xist* clouds in (day 6) EB-differentiated *Rlim*KOp ESCs in RNA FISH using *Xist* as the probe. Representative images are shown.

(D) Summary of three independent experiments as shown in (C). *Xist* clouds in ESCs of 10 EBs were evaluated, with >100 cells counted per EB. Error bars indicate SEM.

RLIM340, as opposed to dominant-negative functions. Consistent with findings that substrate proteins are often targeted by multiple E3 ligases mediated by interactions via the same or a similar binding site (Bach and Ostendorff, 2003; Güngör et al., 2007), these results provide additional evidence that varying levels or the repertoire of cellular competence factors in different ESC systems influences cellular REX1 levels and XCI.

Efficiency of *Rlim*-Independent XCI *In Vitro* Is Influenced by Culture Conditions

Although the lack of RLIM does not affect overall rXCI efficiency *in vivo* (Figures 1 and S1), when compared to WT, *Rlim*KO ESCs undergo XCI with reduced efficiency upon EB differentiation *in vitro* (Figure 2), suggesting suboptimal culture conditions. In utero, ESCs differentiate in the context of extraembryonic cells and mammalian embryos are exposed to low O_2 levels (2%–8%) (Fischer and Bavister, 1993). We therefore tested whether XCI efficiency of *Rlim*KO ESCs could be improved by mimicking these natural conditions. To test possible influences of extraembryonic cell types on XCI, we co-cultured EB-differentiating female GFP-*Rlim*KOp ESCs in the presence of a trophoblast stem cell (TSC) line and/or a primitive endoderm (XEN) cell line (Niakan et al., 2013). However, this approach yielded no signs of improved XCI (data not shown). To examine influences of O_2 levels on XCI, we compared *Xist* RNA levels and formation of clouds in *Rlim*KO ESCs with WTp ESCs, differentiated by EB and cultured in 7.5% O_2. EB differentiation in 7.5% O_2 resulted in a general increase of around 2-fold in *Xist* levels and *Xist* cloud

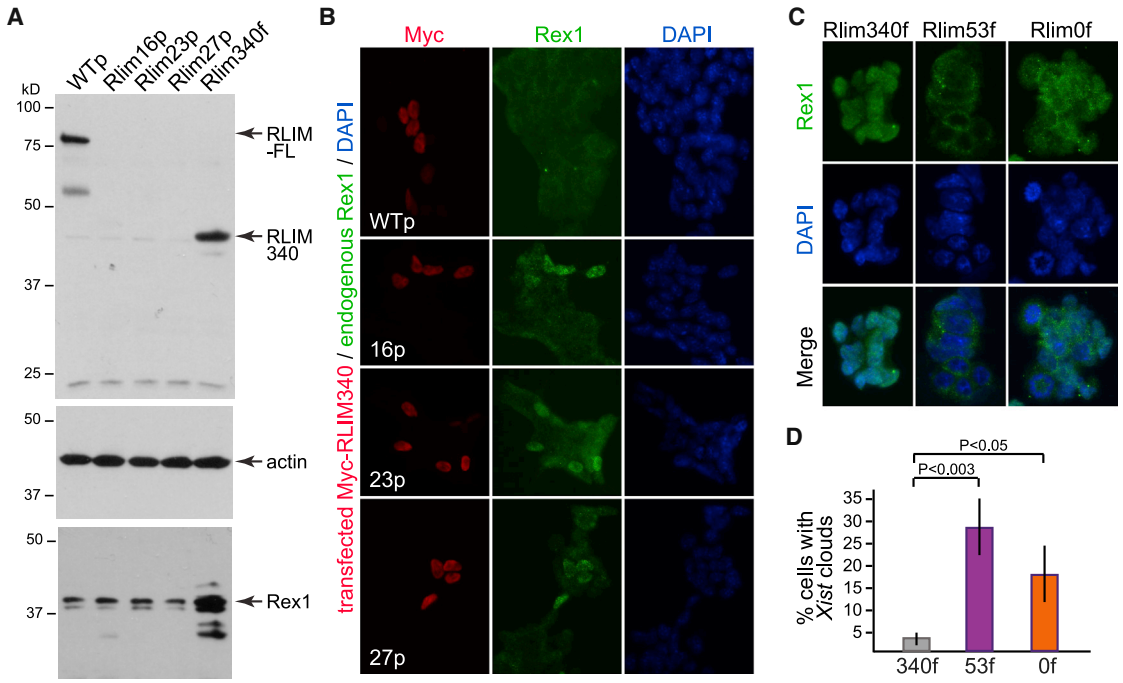

Figure 3. Truncated RLIM340 Protein Is Expressed in *Rlim*340f ESCs

(A) Western blot on undifferentiated ESCs was consecutively hybridized with RLIM middle region (RLIM-M), β-actin, and REX1 antibodies. Note the presence of RLIM340 in *Rnf12*KO (*Rlim*340f) ESCs. Moreover, REX1 levels are elevated in *Rlim*340f ESCs, but not in *Rlim*KOp ESCs.

(B) Forced expression of Myc-tagged RLIM340 in *Rlim*KOp ESCs leads to nuclear accumulation of endogenous REX1.

(C) RLIM340 traps REX1 in the nucleus. ICC on undifferentiated ESCs using REX1 antibodies. Note mostly nuclear localization of REX1 in *Rlim*340f ESCs, but not in *Rlim*53f and *Rlim*0f ESCs.

(D) Presence of RLIM340 inhibits XCI efficiency. Summary of *Xist* clouds from three independent experiments in *Rlim*340f, *Rlim*53f, and *Rlim*0f ESCs EB differentiated for 6 days. From each experiment, *Xist* clouds in ESCs of 10 EBs were evaluated, with >100 cells counted per EB.

Error bars indicate SEM. See also Figure S2.

development in all *Rlim*KO ESC lines (Figures 4A–4D) (data not shown). Although at day 6 of differentiation *Rlim*16p ESCs appeared to develop similar XCI efficiencies when compared to WT, efficiency was lower at day 3 of EB differentiation (Figure S3A). No effects of 7.5% O_2 on XCI efficiency were observed on day 6 RA-differentiated *Rlim*KO ESCs (data not shown). Transcriptome analyses of undifferentiated and day 6 EB-differentiated WTp, *Rlim*16p, and E14 male ESCs via RNA sequencing (RNA-seq) confirmed similar *Xist* levels in female ESCs (Figure S3B), and comparisons of total X-linked transcripts versus total autosomal transcripts in differentiating WTp and mutant female ESC lines (relative to male E14) revealed similar global X silencing in *Rlim*KOp and WTp ESCs (Figures 4E and S3C). Because iXCI in female mice is *Rlim*-dependent, whereas rXCI occurs in an *Rlim*-independent fashion, the identification of *Rlim*-dependent and *Rlim*-independent pathways for XCI in female ESCs illuminates mechanisms underlying X dosage compensation in female mice, including the epigenetic swtch from iXCI to rXCI in epiblast cells (Figure 4F).

DISCUSSION

Investigating XCI in female ESCs, we found that in an *in vivo* context, XCI in ESCs lacking *Rlim* occurs with efficiencies similar to those in WT ESCs (Figure 1), but *in vitro Rlim*-independent XCI is highly sensitive to the differentiation protocol, as well as cell culture conditions (Figures 2 and 4). In particular, XCI in RA-differentiated ESCs is strictly *Rlim*-dependent (Figure 2), indicating that this type of differentiation is not compatible with *Rlim*-independent XCI. The formation of EBs more closely mimics the situation in blastocysts, and the finding that RLIM levels slightly increase during EB differentiation (Figure 2A) (Marks et al., 2015) is reminiscent of the increase in *Rlim* mRNA levels observed in early blastocysts, when the ICM forms (Wang et al., 2016). Moreover, we found that culturing differentiating ESCs in 7.5% O_2 levels had a general positive effect on *Rlim*-independent XCI efficiency (Figure 4). In utero, mammalian embryos are naturally exposed to low 2%–8% O_2 levels (Fischer and Bavister, 1993), and atmospheric O_2 levels negatively influence development, global gene expression, and XCI in cultured embryos or ESCs (Harvey et al., 2004; Lengner et al., 2010; Orsi and Leese, 2001). However, even in 7.5% O_2, the kinetics of XCI in *Rlim*KO cells is still slower than in WT ESCs (Figure S3A), suggesting that these remain suboptimal XCI conditions. An alternative possibility is that the *Rlim*-independent XCI occurs more slowly upon induction of ESC differentiation. In this scenario, the presence of RLIM facilitates the more rapid XCI kinetics in WT ESCs.

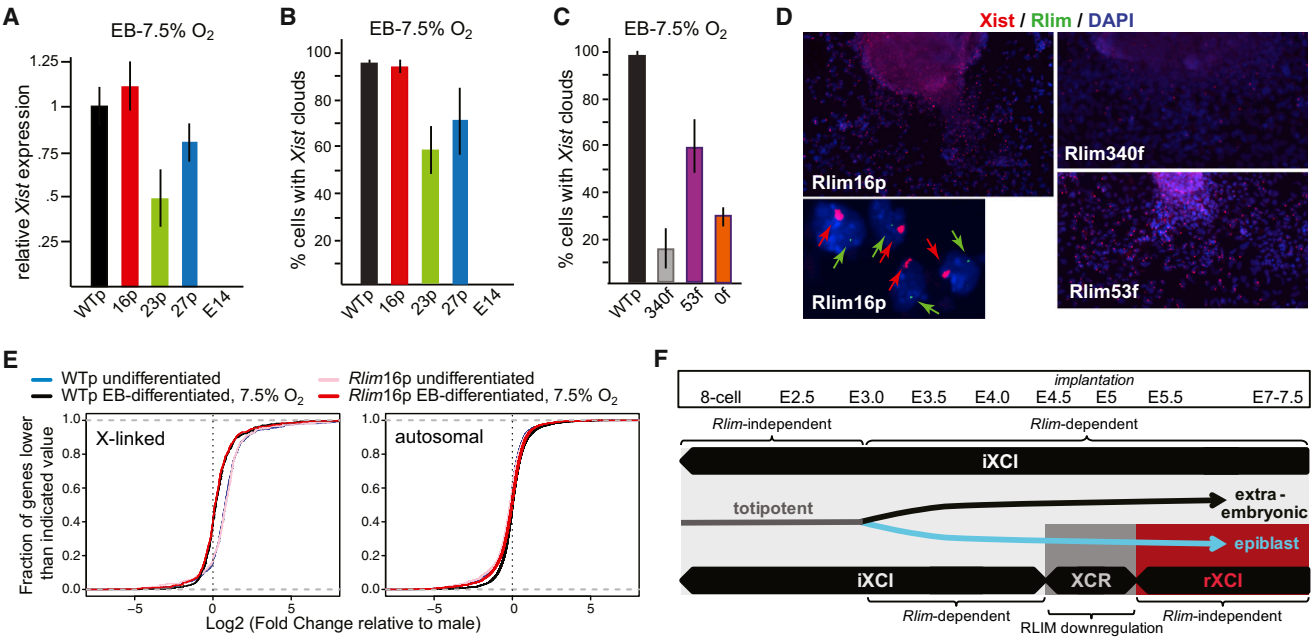

Figure 4. RLIM-Independent XCI in ESCs *In Vitro*

(A) *Xist* levels (ssqRT-PCR) in ESCs, EB differentiated and cultured for 6 days in 7.5% O_2. Results represent three independent experiments. *Xist* levels of differentiated WTp cells are set to 1.

(B and C) Summary of comparison of *Xist* cloud formation ESCs (EB-differentiated in 7.5% O2) cultured for 6d as determined by RNA FISH using *Xist* as probe. Genotypes are indicated. Shown are *Rlim*KO ESCs in PGK12.1 background (B) or F121 background (C). *Xist* clouds were counted in two independent experiments (10 EBs with >100 cells counted per EB).

(D) Representative images of RNA FISH on day 6 EB-differentiated ESCs (7.5% O_2). The lower-left panel shows *Rlim*16p co-hybridized with *Xist* (red) and *Rlim* (green) probes in higher magnification.

(E) *Rlim*-independent chromosome-wide X silencing *in vitro*. Log2-transformed RNA-seq data obtained from two biological replicates each of undifferentiated and differentiated (day 6 EB differentiation; 7.5% O_2) WT, *Rlim*16p, and E14 ESCs were compared for female versus male (F/M) expression level ratios from 550 X-linked genes (left panel) and 13,526 autosomal genes (right panel).

(F) Summary of XCI during female mouse embryogenesis and dependence on *Rlim*. Embryonic stages iXCI (light gray), rXCI (red), and XCR (dark gray), as well as embryonic cell lineages, are indicated (gray, totipotent cell lineage; black, extraembryonic cell lineage; blue, epiblast cell lineage).

Error bars in (A)–(C) indicate SEM. See also Figure S3.

Combined, our results indicate elevated XCI efficiencies by the *Rlim*-independent pathway under conditions that more closely parallel conditions found *in vivo*. Thus, it will be interesting to identify the factor or factors and conditions that orchestrate rXCI in epiblasts.

In contrast to epiblast cells of embryos undergoing rXCI, RLIM expression is maintained in differentiating ESCs (Figure 2A). Thus, the *Rlim*-dependent pathway likely contributes to XCI to varying degrees *in vitro*, depending on differentiation, culture conditions, and likely the specific ESC model used. The findings that (1) REX1 levels are not significantly affected by the *Rlim* deletion in PGK12.1 ESCs (Figure 3A), (2) REX1 levels rapidly drop to undetectable levels within 24 hr of RA differentiation in ESCs (Gontan et al., 2012) (data not shown), and (3) the development of *Xist* clouds and H3K27me3 foci upon RA differentiation is strictly *Rlim*-dependent (Figures 1B and 1C) indicate that at least some functions of *Rlim* for XCI occur independent of REX1. However, the findings that REX1 levels in F121 ESCs are affected by the presence or absence of RLIM (Gontan et al., 2012) and that *Rlim*-independent XCI in these ESCs is generally less efficient when compared to PGK12.1 ESCs (Figures 4A–4D) suggests that the cellular repertoire of expressed competency factors (e.g., E3 ligases) in different female ESC models has an important impact on XCI *in vitro*.

*Rlim*340f ESCs exhibit very low XCI activity, and our results suggest that expression of the truncated RLIM340 might be a contributing factor, because it traps REX1 in the nucleus (Figure 3), and overall REX1 levels are strongly affected by RLIM in F121 ESCs (Gontan et al., 2012), but not in PGK12.1 ESCs (Figure 3). Because RLIM regulates a variety of factors by both RING-finger-dependent and RING-finger-independent mechanisms (Her and Chung, 2009; Krämer et al., 2003; Ostendorff et al., 2002), it is likely that the activities of other nuclear proteins are altered in *Rlim*340f ESCs, with a potential effect on XCI. Moreover, the specific epigenetic background in individual ESC lines may contribute to XCI activity, because *Rlim*KO ESC lines undergo XCI with variable efficiencies. Although it is clear that RLIM promotes XCI, our results indicate that *in vivo*, additional factors must be involved in proper counting of X chromosomes, as previously proposed (Barakat et al., 2011; Jonkers et al., 2009). However, secondary roles for *Rlim* in rXCI in counting X's in mice with X chromosome abnormalities

cannot be ruled out. In this context, it is important to point out the possibility that the gain-of-function activity of RLIM340 might contribute to the skewed inactivation of the X harboring the mutated *Rlim* allele in *Rlim*340f heterozygous ESCs (Jonkers et al., 2009).

During mouse embryogenesis, RLIM protein is detectable throughout preimplantation development, consistent with its functions in iXCI maintenance. However, in contrast to differentiating ESCs in culture (Figure 2A), RLIM protein levels are downregulated in nuclei of epiblast cells of implanting embryos to levels that are undetectable by immunofluorescence (Shin et al., 2014). RLIM levels continue to remain low at early post-implantation stages through E7.5. At E8.5, RLIM protein levels are slowly upregulated in specific embryonic cell types, and by E11.5, RLIM protein is widely detectable in many tissues (Ostendorff et al., 2006) (data not shown). Thus, functions of *Rlim* in Xi maintenance at later embryonic stages and/or in mature tissue types are likely. The developmental expression pattern, combined with the finding of *Rlim*-dependent and *Rlim*-independent XCI pathways in ESCs *in vitro*, suggests a model for X dosage compensation in which Rlim occupies a major role to maintain *Xist* clouds and iXCI in cells of female embryos before X chromosome reactivation (XCR) (Figure 4F). Although this role continues in extraembryonic tissues, RLIM is specifically downregulated in the epiblast lineage shortly before implantation, thereby likely contributing to XCR, followed by induction of rXCI by an *Rlim*-independent pathway (Figure 4F). This scenario is consistent with findings that *Rlim* is essential for the maintenance of iXCI but dispensable for rXCI in epiblast cells. Moreover, it explains the precocious rXCI in epiblast cells of Δ/Δ blastocyst outgrowths (Figure 1A), because with lack of iXCI, XCR is not required before induction of rXCI. Thus, iXCI in early female embryos and rXCI in epiblast cells are regulated by distinct pathways, and the existence of Rlim-dependent and *Rlim*-independent pathways for XCI in female ESCs is likely the consequence of persistent RLIM expression upon differentiation *in vitro*.

EXPERIMENTAL PROCEDURES

Cell Culture and Generation of PGK12.1 Cell Lines Lacking RLIM

Female PGK12.1 and male E14 ESCs were cultured as described (Hooper et al., 1987; Norris et al., 1994). For RA differentiation, cells were plated at 2.5 × 10^4/cm^2 and cultured minus Leukemia inhibitory factor (LIF) with 100 nM RA (Sigma R2625) for 6 days. EBs were formed in suspension by incubating cells in medium lacking LIF for 3 days on bacteriological Petri dishes, and after selection of smooth, spherical EBs, cells were differentiated attached to tissue culture dishes for the specified times. *Rlim*−/− PGK12.1 cell lines were generated by CRISPR/Cas9 cleavage (Cong et al., 2013; Mali et al., 2013) in exon 3. PGK12.1 cells were electroporated with pX330 (Cong et al., 2013) containing a puromycin resistance cassette for clonal selection, into which guide RNA oligonucleotides were cloned. Homozygous null mutations were confirmed by sequencing. GFP lines were generated by infection with pWPT-GFP lentivirus (Addgene). ESCs with a KO of RLIM340 (*Rlim*53f and *Rlim*0f) were generated based on Rnf12KO ESCs (Barakat et al., 2011) as described earlier, except that pX330 with a hygromycin resistance cassette was used. Cells were cultured in 7.5% O_2 in a hypoxic chamber.

Oligonucleotides and RT-qPCR

Oligonucleotides used in this study are summarized in Table S1. For ssqRT-PCR, RNA was isolated using TRIzol (Ambion) and treated with DNase1 (New England Biolabs). cDNA was synthesized with reverse transcriptase and primers specific for *Xist* and *Gapdh*. qPCR was performed with KAPA SYBR FAST Universal qPCR Master Mix on an Eppendorf realplex^2. The absence of genomic DNA was verified in RT-minus reactions.

Generation of Chimeric Mouse Embryos and Preparation of MEFs

E3.5 blastocysts (C57BL/6J-Tyrc-2J/J strain) were microinjected with 12–15 individual ESCs. Injected blastocysts were surgically transferred into the uteri of pseudo-pregnant recipient SWR/J mouse strain (SW) female mice. After recovery, the females were housed under standard vivarium conditions. Pregnant dams were sacrificed 10 days post-surgery, and chimeric E12.5 embryos were recovered for preparation of MEFs (Shin et al., 2010). All mice were housed in the animal facility of the University of Massachusetts Medical School (UMMS) and used according to NIH guidelines and those established by the UMMS Institute of Animal Care and Usage Committee.

Blastocyst Outgrowths and RNA FISH

Mice were maintained on a C57BL/6 background, and parental genotypes to generate embryos for blastocyst outgrowths were based on described mouse models (Shin et al., 2010, 2014). E4 blastocysts were generated by natural mating, cultured for 48–96 hr before RNA FISH, and genotyped after image recording. All mice were housed in the animal facility of UMMS and used according to NIH guidelines and those established by the UMMS Institute of Animal Care and Usage Committee. RNA FISH experiments including probes have been described (Shin et al., 2010, 2014). The *Rlim* probe detects mRNAs transcribed from both WT and KO alleles (Shin et al., 2010).

Antibodies, Western Blots, Immunostaining, and Transient Transfections

Primary antibodies were rabbit and guinea pig RLIM (Ostendorff et al., 2002, 2006), H3K27me3 (Abcam ab6002 and Millipore 07-447), GFP (Rockland 600-101-215), REX1 (Abcam ab28141), Myc (Sigma 9E10), OCT4 (Santa Cruz sc-8628), and β-actin (Sigma A1978 and A5316). Secondary antibodies were Alexa Fluor 488 donkey anti-rabbit immunoglobulin G (IgG) (Invitrogen, A21206), Alexa Fluor 488 goat anti-mouse IgG (Invitrogen, A11029), Alexa Fluor 546 goat anti-guinea pig IgG (Invitrogen A11074), Alexa Fluor 568 goat anti-rabbit IgG (Invitrogen, A11011), goat anti-rabbit IgG-horseradish peroxidase (HRP) (Bio-Rad 170-6515), goat anti-mouse IgG-HRP (Bio-Rad 170-6516), and donkey anti-goat IgG-HRP (Santa Cruz sc-2020). Whole-cell lysates for western blots were prepared by lysing cells in WE16th lysis buffer (25 mM Tris [pH 7.5], 125 mM NaCl, 2.5 mM EDTA, 0.05% SDS, 0.5% NP-40, 10% glycerol). Transient transfections of RLIM340 (in pCS2MT) were carried out using FuGENE HD Transfection Reagent (Promega).

RNA-Seq and Data Analyses

RNA-seq on ESC lines was essentially performed as described (Vallaster et al., 2017), and libraries were sequenced on a NextSeq 500 platform from Illumina. Quality-controlled reads were aligned to the mouse genome (*Mus musculus*/mm10) using TopHat (v.2.0.12) (Trapnell et al., 2009), with default settings, except that parameter read mismatches were set to 2, followed by running HTSeq (v.0.6.1p1) (Anders et al., 2015) and Bioconductor packages edgeR (v.3.10.0) (Robinson et al., 2010; Robinson and Smyth, 2007), for differential gene expression analysis, and ChIPpeakAnno (v.3.2.0) (Zhu, 2013), for annotation. edgeR and trimmed mean of M value (TMM) were used as described (Wang et al., 2016).

Statistical Analyses

Student's t tests were used to calculate statistical differences between individual groups via Microsoft Excel. p values < 0.05 were considered statistically significant.

DATA AND SOFTWARE AVAILABILITY

The accession number for the RNA-seq data reported in this paper is GEO: GSE101838.

SUPPLEMENTAL INFORMATION

Supplemental Information includes three figures and one table and can be found with this article online at https://doi.org/10.1016/j.celrep.2017.12.004.

ACKNOWLEDGMENTS

We are grateful to M. Green and S. Bhatnagar for providing PGK12.1 ESCs, J. Gribnau and C. Gontan for providing Rnf12KO (*Rlim*340f) ESCs, and K. Hadjantonakis for providing TSCs and XEN cells. We thank M. Keeler for assistance in the UMMS Transgenic Animal Modeling Core and S. Sissaoui and N. Lawson for the pWPT-GFP vector. This work was supported from NIH grants R01CA131158 (to I.B.), R01HD072122 (to T.G.F.), R01HD080224 and DP1ES025458 (to O.J.R.), R01CA077735 (to S.N.J.), and R01GM053234 (to J.B.L.).

AUTHOR CONTRIBUTIONS

Conceptualization: I.B. and F.W.; Methodology: F.W., K.N.M., A.B., J.Y., J.S., J.G., M.B., and X.Z.; Investigation, F.W., K.N.M., A.B., J.Y., J.S., J.G., M.B., X.Z., and I.B.; Supervision: I.B., T.G.F., O.J.R., S.N.J., L.J.Z., and J.B.L.; Writing: I.B., F.W., K.N.M., and T.G.F.

DECLARATION OF INTERESTS

The authors declare no competing interests.

Received: August 18, 2017
Revised: November 2, 2017
Accepted: December 1, 2017
Published: December 26, 2017

REFERENCES

Anders, S., Pyl, P.T., and Huber, W. (2015). HTSeq—a Python framework to work with high-throughput sequencing data. Bioinformatics *31*, 166–169.

Bach, I., and Ostendorff, H.P. (2003). Orchestrating nuclear functions: ubiquitin sets the rhythm. Trends Biochem. Sci. *28*, 189–195.

Bach, I., Rodriguez-Esteban, C., Carrière, C., Bhushan, A., Krones, A., Rose, D.W., Glass, C.K., Andersen, B., Izpisúa Belmonte, J.C., and Rosenfeld, M.G. (1999). RLIM inhibits functional activity of LIM homeodomain transcription factors via recruitment of the histone deacetylase complex. Nat. Genet. *22*, 394–399.

Barakat, T.S., Gunhanlar, N., Pardo, C.G., Achame, E.M., Ghazvini, M., Boers, R., Kenter, A., Rentmeester, E., Grootegoed, J.A., and Gribnau, J. (2011). RNF12 activates Xist and is essential for X chromosome inactivation. PLoS Genet. *7*, e1002001.

Barakat, T.S., Loos, F., van Staveren, S., Myronova, E., Ghazvini, M., Grootegoed, J.A., and Gribnau, J. (2014). The trans-activator RNF12 and cis-acting elements effectuate X chromosome inactivation independent of X-pairing. Mol. Cell *53*, 965–978.

Cong, L., Ran, F.A., Cox, D., Lin, S., Barretto, R., Habib, N., Hsu, P.D., Wu, X., Jiang, W., Marraffini, L.A., and Zhang, F. (2013). Multiplex genome engineering using CRISPR/Cas systems. Science *339*, 819–823.

Fischer, B., and Bavister, B.D. (1993). Oxygen tension in the oviduct and uterus of rhesus monkeys, hamsters and rabbits. J. Reprod. Fertil. *99*, 673–679.

Gontan, C., Achame, E.M., Demmers, J., Barakat, T.S., Rentmeester, E., van IJcken, W., Grootegoed, J.A., and Gribnau, J. (2012). RNF12 initiates X-chromosome inactivation by targeting REX1 for degradation. Nature *485*, 386–390.

Güngör, C., Taniguchi-Ishigaki, N., Ma, H., Drung, A., Tursun, B., Ostendorff, H.P., Bossenz, M., Becker, C.G., Becker, T., and Bach, I. (2007). Proteasomal selection of multiprotein complexes recruited by LIM homeodomain transcription factors. Proc. Natl. Acad. Sci. USA *104*, 15000–15005.

Harvey, A.J., Kind, K.L., Pantaleon, M., Armstrong, D.T., and Thompson, J.G. (2004). Oxygen-regulated gene expression in bovine blastocysts. Biol. Reprod. *71*, 1108–1119.

Her, Y.R., and Chung, I.K. (2009). Ubiquitin ligase RLIM modulates telomere length homeostasis through a proteolysis of TRF1. J. Biol. Chem. *284*, 8557–8566.

Hooper, M., Hardy, K., Handyside, A., Hunter, S., and Monk, M. (1987). HPRT-deficient (Lesch-Nyhan) mouse embryos derived from germline colonization by cultured cells. Nature *326*, 292–295.

Jiao, B., Taniguchi-Ishigaki, N., Güngör, C., Peters, M.A., Chen, Y.W., Riethdorf, S., Drung, A., Ahronian, L.G., Shin, J., Pagnis, R., et al. (2013). Functional activity of RLIM/Rnf12 is regulated by phosphorylation-dependent nucleocytoplasmic shuttling. Mol. Biol. Cell *24*, 3085–3096.

Jonkers, I., Barakat, T.S., Achame, E.M., Monkhorst, K., Kenter, A., Rentmeester, E., Grosveld, F., Grootegoed, J.A., and Gribnau, J. (2009). RNF12 is an X-encoded dose-dependent activator of X chromosome inactivation. Cell *139*, 999–1011.

Krämer, O.H., Zhu, P., Ostendorff, H.P., Golebiewski, M., Tiefenbach, J., Peters, M.A., Brill, B., Groner, B., Bach, I., Heinzel, T., and Göttlicher, M. (2003). The histone deacetylase inhibitor valproic acid selectively induces proteasomal degradation of HDAC2. EMBO J. *22*, 3411–3420.

Lengner, C.J., Gimelbrant, A.A., Erwin, J.A., Cheng, A.W., Guenther, M.G., Welstead, G.G., Alagappan, R., Frampton, G.M., Xu, P., Muffat, J., et al. (2010). Derivation of pre-X inactivation human embryonic stem cells under physiological oxygen concentrations. Cell *141*, 872–883.

Mali, P., Yang, L., Esvelt, K.M., Aach, J., Guell, M., DiCarlo, J.E., Norville, J.E., and Church, G.M. (2013). RNA-guided human genome engineering via Cas9. Science *339*, 823–826.

Marks, H., Kerstens, H.H., Barakat, T.S., Splinter, E., Dirks, R.A., van Mierlo, G., Joshi, O., Wang, S.Y., Babak, T., Albers, C.A., et al. (2015). Dynamics of gene silencing during X inactivation using allele-specific RNA-seq. Genome Biol. *16*, 149.

Niakan, K.K., Schrode, N., Cho, L.T., and Hadjantonakis, A.K. (2013). Derivation of extraembryonic endoderm stem (XEN) cells from mouse embryos and embryonic stem cells. Nat. Protoc. *8*, 1028–1041.

Norris, D.P., Patel, D., Kay, G.F., Penny, G.D., Brockdorff, N., Sheardown, S.A., and Rastan, S. (1994). Evidence that random and imprinted Xist expression is controlled by preemptive methylation. Cell *77*, 41–51.

Orsi, N.M., and Leese, H.J. (2001). Protection against reactive oxygen species during mouse preimplantation embryo development: role of EDTA, oxygen tension, catalase, superoxide dismutase and pyruvate. Mol. Reprod. Dev. *59*, 44–53.

Ostendorff, H.P., Peirano, R.I., Peters, M.A., Schlüter, A., Bossenz, M., Scheffner, M., and Bach, I. (2002). Ubiquitination-dependent cofactor exchange on LIM homeodomain transcription factors. Nature *416*, 99–103.

Ostendorff, H.P., Tursun, B., Cornils, K., Schlüter, A., Drung, A., Güngör, C., and Bach, I. (2006). Dynamic expression of LIM cofactors in the developing mouse neural tube. Dev. Dyn. *235*, 786–791.

Payer, B. (2016). Developmental regulation of X-chromosome inactivation. Seminars in cell & developmental biology *56*, 88–99.

Robinson, M.D., and Smyth, G.K. (2007). Moderated statistical tests for assessing differences in tag abundance. Bioinformatics *23*, 2881–2887.

Robinson, M.D., McCarthy, D.J., and Smyth, G.K. (2010). edgeR: a Bioconductor package for differential expression analysis of digital gene expression data. Bioinformatics *26*, 139–140.

Shin, J., Bossenz, M., Chung, Y., Ma, H., Byron, M., Taniguchi-Ishigaki, N., Zhu, X., Jiao, B., Hall, L.L., Green, M.R., et al. (2010). Maternal Rnf12/RLIM

is required for imprinted X-chromosome inactivation in mice. Nature *467*, 977–981.

Shin, J., Wallingford, M.C., Gallant, J., Marcho, C., Jiao, B., Byron, M., Bossenz, M., Lawrence, J.B., Jones, S.N., Mager, J., and Bach, I. (2014). RLIM is dispensable for X-chromosome inactivation in the mouse embryonic epiblast. Nature *511*, 86–89.

Trapnell, C., Pachter, L., and Salzberg, S.L. (2009). TopHat: discovering splice junctions with RNA-seq. Bioinformatics *25*, 1105–1111.

Vallaster, M.P., Kukreja, S., Bing, X.Y., Ngolab, J., Zhao-Shea, R., Gardner, P.D., Tapper, A.R., and Rando, O.J. (2017). Paternal nicotine exposure alters hepatic xenobiotic metabolism in offspring. eLife *6*, e24771.

Wang, F., Shin, J., Shea, J.M., Yu, J., Bošković, A., Byron, M., Zhu, X., Shalek, A.K., Regev, A., Lawrence, J.B., et al. (2016). Regulation of X-linked gene expression during early mouse development by Rlim. eLife *5*, e19127.

Zhu, L.J. (2013). Integrative analysis of ChIP-chip and ChIP-seq dataset. Methods Mol. Biol. *1067*, 105–124.